Available online at www.sciencedirect.com

SciVerse ScienceDirect

Ceramics International 38 (2012) 3935–3942

CERAMICS INTERNATIONAL

www.elsevier.com/locate/ceramint

Crystal structure refinement of $Bi_{1-x}Nd_xFeO_3$ multiferroic by the Rietveld method

Ashwini Kumar, Dinesh Varshney *

School of Physics, Vigyan Bhawan, Devi Ahilya University, Khandwa Road Campus, Indore 452001, India

Received 19 December 2011; accepted 17 January 2012
Available online 25 January 2012

Abstract

The effect of Nd doping on $Bi_{1-x}Nd_xFeO_3$ (x = 0.0, 0.175, 0.20) multiferroics synthesized by chemical co-precipitation method has been investigated by Rietveld analysis of X-ray powder diffraction (XRD) data. The formations of the single-phase compounds were confirmed by XRD. X-ray diffraction along with the Rietveld-refinement showed a gradual change in crystal structure from rhombohedral to triclinic with increasing Nd doping concentration. The bond distances along with bond angles between atoms for all the compounds were calculated which supports the structural results. Raman spectroscopy also recommends a structural change and is accompanied by the weakening of long-range ferroelectric order with increasing doping concentration (x). The results of Raman spectra for $BiFeO_3$ (BFO) match well with the earlier reported bulk ceramic and epitaxially grown thin film of BFO. The ferroelectric-paraelectric transition in 20% Nd BFO substituted was explained according to the change of Bi–O covalent bond as a result of decline of stereochemical activity of Bi lone pair electron and is further confirmed through ferroelectric polarization (P–E) hysteresis loop.

Keywords: A. Powders: chemical preparation; B. X-ray methods; C. Ferroelectric properties; D. Perovskites; E. Structural applications

1. Introduction

Multiferroics have been an object of immense interest due to coexistence of two or more of the possible ferroic orders occur simultaneously in single-phase material [1]. The multiferroism is focused due to their wide range of potential applications, including information-storage device, spintronics, magneto-electric sensor devices, and multiple-state memories [2]. Among various multiferroic materials investigated so far, $BiFeO_3$ is widely studied due to coupling between ferroelectric and magnetic order at room temperature and causing possibility of room temperature multiferroic devices. $BiFeO_3$ has a rhombo-hedrally distorted perovskite structure (space group $R3c$) with chemical formula ABO_3 and its high Curie temperature ($T_C \sim 1083$ K) [3]. The ferroelectricity in $BiFeO_3$ is attributed to the Bi^{3+} $6s^2$ lone pair electrons, whereas magnetism is believed to originate from partially filled d orbital of Fe [4]. It simultaneously shows G-type canted anti-ferromagnetic order below (T_N = 675 K) with a spatially modulated spiral spin structure [5,6].

It has been noticed that partial substitution of rare-earth elements like La, Nd, and Ho at the Bi site in BFO helps in eliminating the secondary (impurity) phase along with a structural phase transformation and improving the ferroelectric and ferromagnetic properties. Yuan et al. reported a structural transformation from rhombohedral structure for $BiFeO_3$ to triclinic structure for $Bi_{1-x}Nd_xFeO_3$ (x = 0.05–0.15) and the magnetoelectric coupling was clear in $Bi_{1-x}Nd_xFeO_3$ (x = 0.15–0.175) near the Néel temperature of ~653 K whereas, for further Nd doped samples $Bi_{1-x}Nd_xFeO_3$ (x = 0.175–0.2) a pseudotetragonal structure has been reported [7]. Similar author have reported a structural transformation from rhombohedral to monoclinic structure for $Bi_{1-x}Nd_xFeO_3$ (x = 0–0.15) ceramic prepared by an improved rapid liquid phase sintering method [8]. Jeon et al. have studied the effect of Ho doping on Pure BFO bulk ceramic and concluded that with Ho doping the remnant polarization and switching characteristic was improved at low field by reducing the leakage current. Additionally the ferromagnetic properties were also enhanced by Ho doping [9]. These improved properties obtained by rare

* Corresponding author. Tel.: +91 731 2467028; fax: +91 731 2465689.
E-mail address: vdinesh33@rediffmail.com (D. Varshney).

0272-8842/$36.00
doi:10.1016/j.ceramint.2012.01.046

earth doping demonstrate the possibility of enhancing the multiferroic applicability of BFO.

From the existing literature it has been observed that different authors have tried to investigate, analyze, and comprehend the anomalous physical behavior using different experimental techniques but still need further improvements. Because of the technological importance and interesting physical properties, it is necessary to be aware of the crystal structure of these compounds. Motivated with these in this present work, we prepare Nd doped $BiFeO_3$ ceramic i.e. $Bi_{1-x}Nd_xFeO_3$ (x = 0.0, 0.175, 0.20) by chemical co-precipitation method. A detailed structural analysis using the Rietveld refinement method has been reported and studied the effect of Nd substitution at Bi-site in $BiFeO_3$ on structural and ferroelectric properties. In order to reveal the structural transformation the synthesized product was characterized by Raman spectroscopy also. The synthesized samples of $Bi_{1-x}Nd_xFeO_3$ with x = 0.0, 0.175, and 0.20 are further designated as BFO, BNFO-175, and BNFO-20, respectively.

2. Experimental details

The polycrystalline samples of $Bi_{1-x}Nd_xFeO_3$ with x = 0.0, 0.175, and 0.20 (abbreviated as BFO, BNFO-175, and BNFO-20, respectively) used in this investigation were prepared using a chemical co-precipitation method, and starting materials with a purity at least 99% or higher. The chemical reagents for this experiment $Bi(NO_3)_3{\cdot}5H_2O$, $Fe(NO_3)_3{\cdot}9H_2O$, Nd_2O_3, and sodium hydroxide were used. The deionized water was used during the experiments. The aqueous solution of Bi, Nd, and Fe salts was freshly prepared by taking $Bi(NO_3)_3{\cdot}5H_2O$, $Fe(NO_3)_3{\cdot}9H_2O$, and Nd_2O_3 in appropriate molar ratio. This mixture was heated until the temperature reached 70 °C. On vigorous stirring, the pH of the above solution was raised to 12 rapidly, by the addition of 6 M NaOH. The particles settled at the bottom were collected and the top water layer with excess salts was discarded. The particles have been decanted repeatedly with distilled water to remove salt impurities. Later, the washed particles were dried at room temperature and further calcined at 700 °C for 5 h.

All the samples were characterized by means of X-ray powder diffraction (XRD), Raman spectroscopy, and ferroelectric polarization (P–E) measurement. The XRD measurements were carried out with Cu$K\alpha_1$ (1.5406 Å) radiation using a Bruker D8 Advance X-ray diffractometer. Furthermore, X-ray powder diffraction data were analyzed with Rietveld refinement program. The Raman measurements on as synthesized samples were carried out on Jobin-Yovn Horiba LABRAM (System HR800) spectrometer with a 488 nm excitation source equipped with a Peltier cooled CCD detector (1024 × 256 pixels of 26 microns) and the laser beam was focused on the sample by a 50× lens to give a spot size of 1 μm; the resolution was better than 2 cm^{-1}. After each spectrum had been recorded, a careful visual inspection was performed using white light illumination on the microscope stage in order to detect any change that could have been caused by the laser. Ferroelectric hysteresis (P–E) loop of the samples were measured using RT6000 (Radiant Technologies, USA) at frequency 50 Hz.

3. Rietveld refinement theory

We employed the FullPROF program in the Rietveld analysis; it is intended to refine simultaneously both the structural (lattice cell constants and atomic positions and occupancies) and micro-structural parameters (crystallite size and lattice strain). A detailed description of the mathematical procedures implemented in the Rietveld analysis has been earlier reported [10–13]. Here, we give brief, details of the analysis of experimental powder diffraction patterns done by us. The crystal structure characterization of all the synthesized samples has been made by employing the Rietveld's whole-profile fitting method using FullPROF software [14].

The experimental profiles were fitted with the most suitable pseudo-Voigt analytical function. For both the $K_{\alpha1}$ and $K_{\alpha2}$ profiles, the line broadening function B (2θ) and the symmetric part of instrumental function S (2θ) may be represented by the pseudo-Voigt function:

$$pV(x) = \sum I_{nt}[\eta C(x) + (1-\eta)G(x)] \tag{1}$$

where $C(x) = (1 + x2) - 1$ is the Cauchyian component and $G(x) = \exp[-(\ln 2)x2]$ is the Gaussian component. Considering the integrated intensity of the peaks as a function of structural parameters only, the Marquardt least-squares procedures were adopted for minimization of the difference between the observed and simulated powder diffraction patterns. The minimization was carried out using the reliability index parameter such as the residuals for the weighted pattern R_{wp}, the pattern R_p, Braggs factor R_{Bragg}, structure factor R_F, and goodness of fit χ^2. All these parameters were used as numerical criteria of the quality of the fit of calculated to experimental diffraction data and are represented by relations [15]

$$R_{wp} = \left[\frac{\sum_{i=1,n} w_i\left(y_{i(obs)} - y_{i(cal)}\right)^2}{\sum_{i=1,n} w_i\left(y_{i(obs)}\right)^2}\right]^{1/2} \times 100 \tag{2}$$

$$R_P = \frac{\sum_{i=1,n}\left|y_{i(obs)} - y_{i(cal)}\right|}{\sum_{i=1,n} y_{i(obs)}} \times 100 \tag{3}$$

$$R_{Bragg} = \frac{\sum\left|I_{(obs)} - I_{(cal)}\right|}{\sum\left|I_{(obs)}\right|} \times 100 \tag{4}$$

$$R_{exp} = \left[\frac{n-p}{\sum_{i=1,n} w_i\left(y_{i(obs)}\right)^2}\right]^{1/2} \tag{5}$$

$$\chi^2 = \sum_{i=1,n} \frac{w_i\left(y_{i(obs)} - y_{i(cal)}\right)^2}{n-p+c} \times 100 \tag{6}$$

where $y_{i(obs)}$ is the experimental intensities, $y_{i(cal)}$ is the calculated intensities, $w_i = (1/y_{i(obs)})$ is the weight experimental observations, n is the number of experimental observations, p is the number of fitting parameters, I is the integrated

intensity. The goodness of fit (GOF) is established by comparing R_{wp} with the expected error, R_{exp}. This leads to the value of goodness of fit [16]:

$$\text{GOF} = \frac{R_{wp}}{R_{exp}} \quad (7)$$

Refinements were carried out until convergence was reached and the value of the GOF factor became close to 1 (usually, the final GOF varies from 1.1 to 1.3).

4. Results and discussion

4.1. X-ray diffraction analysis

The X-ray powder diffraction pattern of the $Bi_{1-x}Nd_xFeO_3$ samples with composition $x = 0.0$, 0.175, and 0.20 (abbreviated as BFO, BNFO-175, and BNFO-20, respectively) are shown in Fig. 1. From the XRD pattern, it is observed that pure BFO sample has distorted rhombohedral structure with $R3c$ space group where all the diffraction peaks matches well with the standard crystal data corresponding to the JCPDS file No. 86-1518, except a minor low-intensity impurity peak around $2\theta = 28.42^\circ$ associated with $Bi_2Fe_4O_9$. This impurity peak matches well with the JCPDS file no. 72-1832. Furthermore the diffraction peaks of Nd doped BNFO-175 and BNFO-20 samples revealed triclinic structure ($P1$ space group) matches well with the earlier reported data [7]. It has been noticed that, all the peaks undergo a shift in 2θ with a decrease in peak splitting on increasing the Nd concentration as shown in the inset of Fig. 1.

The shifting of peaks is viewed as a result of replacing the larger Bi^{3+} ion (ionic radii = 1.17 Å [17]) by smaller Nd^{3+} ion (ionic radii = 0.983 Å [17]). This confirms a structural transformation and continual change of lattice constant from rhombohedral structure ($R3c$) to triclinic structure ($P1$). Also the intensity of impurity peak observed at $2\theta = 28.42^\circ$ was found to decrease continuously with Nd-doping and completely disappeared for BNFO-20 sample. This led to the fact that addition of Nd at Bi site is helpful in suppressing the secondary phase. Therefore present samples have a single-phase rhombohedral (BFO) or triclinic (BNFO-175 and BNFO-20) perovskite structure with all constituent components forming a solid solution rather than a mixture of Bi_2O_3, Fe_2O_3, Nd_2O_3 or any other impurity phase except $Bi_2Fe_4O_9$ observed in pure BFO.

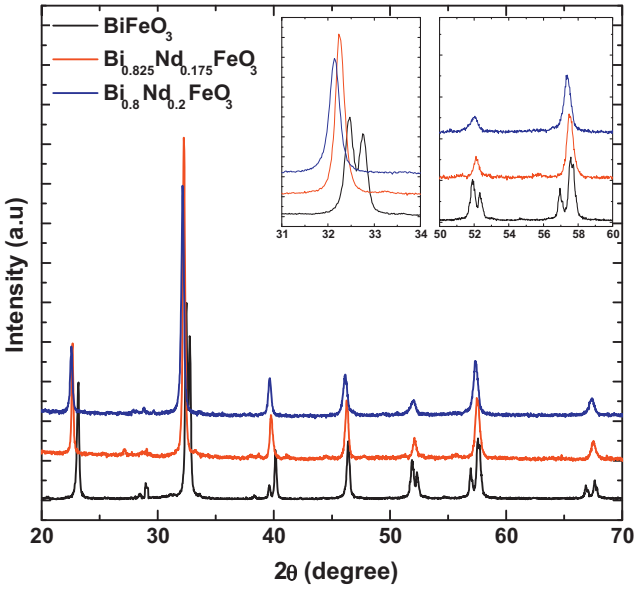

Fig. 1. X-ray powder diffraction (XRD) pattern for $Bi_{1-x}Nd_xFeO_3$ ($x = 0.0$, 0.175, 0.20) samples.

4.2. Refinement of XRD data

In order to further confirm the structural transformation the Rietveld refinement of X-ray powder diffraction pattern for BFO, BNFO-175, and BNFO-20 samples at room temperature was performed using FullPROF program. Rietveld refined XRD pattern is shown in Fig. 2. A pseudo-Voigt function convoluted with an axial divergence symmetry function was

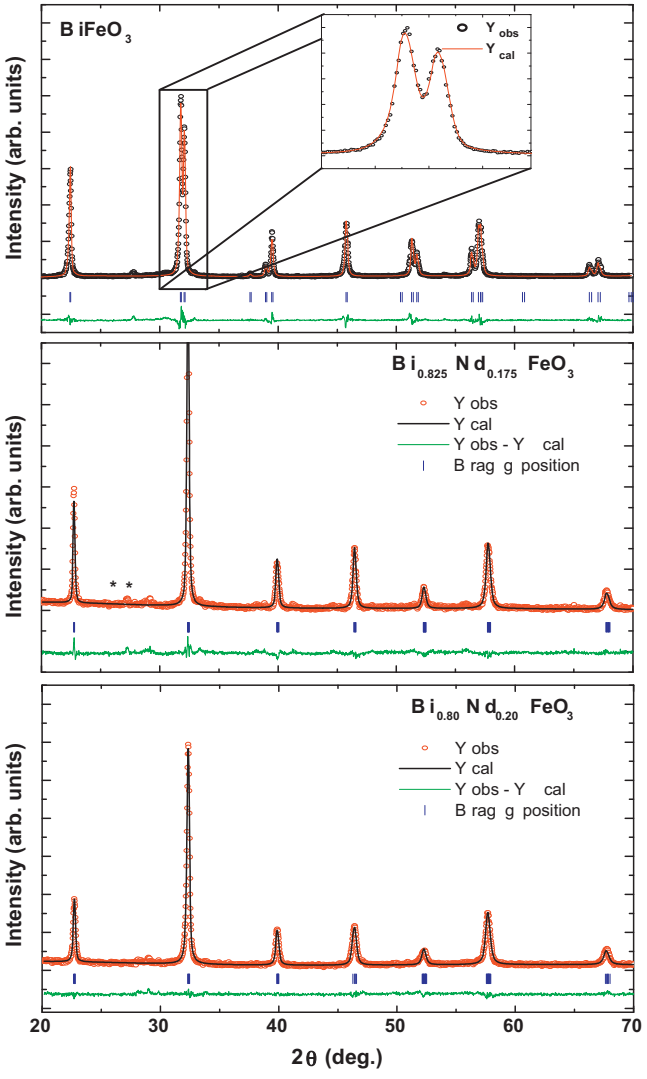

Fig. 2. The Rietveld refinement using FullPROF program for $Bi_{1-x}Nd_xFeO_3$ ($x = 0.0$, 0.175, 0.20) samples.

Table 1
Details of Rietveld refined XRD parameters for $Bi_{1-x}Nd_xFeO_3$ ($x = 0.0, 0.175, 0.2$) samples.

Parameters	$Bi_{1-x}Nd_xFeO_3$		
	$x = 0.0$	$x = 0.175$	$x = 0.20$
2θ range (deg.)	20–70°	20–70°	20–70°
Step size (deg.)	0.02°	0.02°	0.02°
Wavelength	1.5406 Å	1.5406 Å	1.5406 Å
Zero point (2θ,°)	0.1198	−0.0857	−0.1656
Pseudo-Voigt function $pV(x) = \eta C(x) + (1-\eta)G(x)$	$\eta = 0.6321$	$\eta = 0.4529$	$\eta = 0.5533$
Number of refined parameters	25	21	21
Space group	$R3c$	$P1$	$P1$
a (Å)	5.5793	3.9155	3.9162
b (Å)	5.5793	3.9197	3.9211
c (Å)	13.8658	3.9242	3.9229
Volume (Å^3)	373.81	59.67	59.90
R_F	3.26	2.12	2.33
R_{Bragg}	3.91	2.90	2.73
R_{wp}	15.7	14.9	14.5
R_{exp}	8.16	7.10	7.85
R_p	10.6	9.3	9.7
χ^2	3.71	2.45	2.30
GOF	1.32	1.27	1.16

used to model the peak profile of pure $BiFeO_3$ based on space group $R3c$ and Nd doped samples based on $P1$ space group. The lattice parameters and profile parameters were refined but atomic positions and anisotropic displacement parameters were kept fixed to the values earlier reported [18,19]. The stimulated XRD patterns of all the three samples coincide well with the measured XRD pattern with generally small R-values as illustrated in Table 1. The lattice parameters and other refined parameter are also tabulated in Table 1. The atomic coordinates and B_{iso} of all three samples are listed separately in Table 2.

For BFO, both the refined crystal axes ($a = 5.5793$ Å and $c = 13.8658$ Å) and crystal axial angles ($\alpha = \beta = 90°$, $\gamma = 120°$) are found to coincide with those of the rhombohedral $R3c$ symmetry reported elsewhere [18]. While there exist slight differences in the crystal axes of BNFO-175 and BNFO-20, these samples are classified as a special triclinic $P1$ symmetry for BNFO-175 ($a = 3.9155$ Å, $b = 3.9197$ Å, $c = 3.9242$ Å) and for BNFO-20 ($a = 3.9162$ Å, $b = 3.9211$ Å, $c = 3.9229$ Å). The

Table 2
Refined structural parameters for $Bi_{1-x}Nd_xFeO_3$ ($x = 0.0, 0.175, 0.2$) samples.

	x	y	z	B_{iso}
$BiFeO_3$ ($R3c$)				
Bi	0.0000	0.0000	0.2755	1.6222
Fe	0.0000	0.0000	0.0000	0.1245
O	0.6679	0.7647	0.5489	1.8919
$Bi_{0.825}Nd_{0.175}FeO_3$ ($P1$)				
Bi/Nd	0.0000	0.0000	0.0000	1.2571
Fe	0.5690	0.4466	0.5506	1.2240
O1	−0.0805	0.4522	0.6783	0.0342
O2	0.4540	−0.0719	0.6833	1.0142
O3	0.4533	0.4761	0.0175	0.9122
$Bi_{0.80}Nd_{0.20}FeO_3$ ($P1$)				
Bi/Nd	0.0000	0.0000	0.0000	1.2557
Fe	0.5689	0.4362	0.5467	1.2236
O1	−0.0815	0.4542	0.6774	0.0354
O2	0.4538	−0.0722	0.6835	1.0136
O3	0.4541	0.4756	0.0176	0.9215

classification is consistent with the earlier reported data [20]. The stability of perovskite compound based on ABO_3 formula is usually described in terms of Goldschmidt's tolerance factor (t). The tolerance factor for $Bi_{1-x}Nd_xFeO_3$ ($x = 0.0, 0.175, 2.0$) can be written as [21]:

$$t = \frac{[(1-x)R_{Bi^{3+}} + xR_{Nd^{3+}}] + R_{O^{2-}}}{\sqrt{2}[R_{Fe^{3+}} + R_{O^{2-}}]} \quad (8)$$

where $R_{Bi}{}^{3+}$, $R_{Nd}{}^{3+}$, $R_{Fe}{}^{3+}$, $R_O{}^{2-}$ are the effective ionic radii of Bi^{3+}, Nd^{3+}, Fe^{3+}, and O^{2-} ions, respectively. According to Eq. (8), the tolerance factor (t) was found to be 0.888, 0.877, and 0.875 for BFO, BNFO-175, and BNFO-20 compounds, respectively. The 1.3% changes in the value of tolerance factor (t) from BFO to BNFO-20 account for the fact that distortion increases with increasing Nd concentration.

There is a good agreement between observed (obtained from X-ray diagram) and calculated (based on refined cell parameter) interplanner spacing (d-values) of hkl planes and are shown in Table 3. From the table it has been observed that, there is a significant change in the d values for the substituted compound. The significant change in d values may be explained in terms of difference in ionic radii. The structure of

Table 3
Comparison between some of the observed and calculated d-values for $Bi_{1-x}Nd_x FeO_3$ ($x = 0.0, 0.175, 0.20$) samples after Rietveld refinement.

BFO			BNFO-175			BNFO-20		
2θ	d-obs	d-cal	2θ	d-obs	d-cal	2θ	d-obs	d-cal
22.410	3.962	3.964	22.728	3.906	3.909	22.747	3.944	3.906
32.058	2.786	2.789	32.352	2.753	2.764	32.395	2.789	2.761
37.631	2.376	2.388	39.888	2.238	2.258	39.913	2.790	2.569
38.941	2.299	2.310	46.433	1.952	1.954	46.457	2.381	1.953
39.466	1.969	2.281	52.349	1.732	1.746	52.354	2.279	1.746
45.739	1.960	1.982	57.774	1.589	1.594	57.774	1.972	1.594
51.720	1.772	1.766	67.735	1.365	1.382	67.822	1.767	1.380
56.348	1.629	1.631	72.500	1.229	1.302	72.541	1.629	1.302
56.945	1.609	1.615	77.073	1.208	1.236	77.106	1.401	1.235
66.318	1.401	1.408	–	–	–	–	–	–
67.042	1.393	1.394	–	–	–	–	–	–

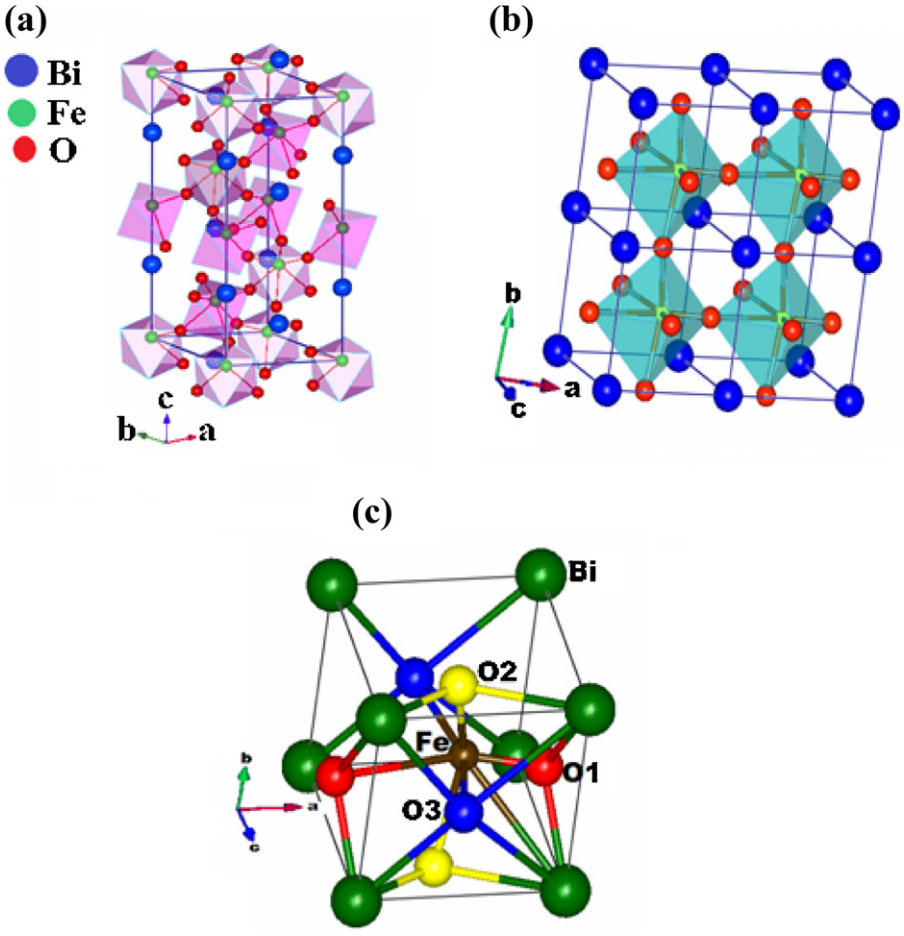

Fig. 3. Generated crystal structure (a) BFO sample representing FeO_6 polyhedron, (b) $Bi_{1-x}Nd_xFeO_3$ samples representing FeO_6 polyhedron, (c) unit cell crystal structure of $Bi_{1-x}Nd_xFeO_3$ samples showing bond representation.

Table 4
Important bond lengths and bond angles of $Bi_{1-x}Nd_xFeO_3$ (0.0, 0.175, 0.2) ceramics.

Compound	Bond type	Bond length (Å)	Bond type	Bond angle (°)
BFO	Bi–Fe	3.067	Fe–O–Fe	150.0
	Bi–O	2.205	O–Bi–O	74.11
	Bi–O	2.462		
	Fe–O	1.885		
	Fe–O	2.2169		
BNFO – 175	Bi/Nd–Fe	2.980	Fe–O1–O3	168.17
	Bi/Nd–O	2.185	Fe–O2–Fe	140.74
	Bi/Nd–O	2.831	Fe–O3–Fe	152.45
	Fe–O	1.901	O1–Bi/Nd–O2	71.47
	Fe–O	2.123	O2–Bi/Nd–O2	113.65
			O1–Bi/Nd–O3	61.99
			O2–Bi/Nd–O3	46.58
BNFO – 20	Bi/Nd–Fe	2.984	Fe–O1–O3	168.16
	Bi/Nd–O	2.196	Fe–O2–Fe	140.83
	Bi/Nd–O	2.835	Fe–O3–Fe	152.46
	Fe–O	1.915	O1–Bi/Nd–O2	71.52
	Fe–O	2.124	O2–Bi/Nd–O2	113.61
			O1–Bi/Nd–O3	61.88
			O2–Bi/Nd–O3	46.63

$Bi_{1-x}Nd_xFeO_3$ ($x = 0.0,\ 0.175,\ 0.20$) compound generated using FullPROF studio program looks like as mentioned in Fig. 3. The ferroic order and spontaneous polarization in BFO mainly results from the Bi^{3+} stereochemically $6s^2$ lone pair electron. Thus it is expected that systematic doping of smaller transition metal or rare earth metal distorts the cation spacing between the oxygen octahedra and alters the long-range ferroelectric order. The ferroelectric properties have a close relation with the Fe–O bond length. The interatomic bond lengths together with the bond angles were calculated by using Bond_Str program. The important bond lengths and bond angles are documented in Table 4. BFO contains a network of oxygen octahedra, where Fe^{3+} cations are inside the octahedra and Bi^{3+} cations fill in between the cavities as shown in Fig. 3. In *R3c* crystal structure the octahedra bond environment is composed of three long degenerate Fe–O bond lengths and three short degenerate Fe–O bond lengths. The FeO_6 octahedron gets distorted due to Nd substitution, resulting change in both bond length and bond angles.

4.3. Raman analysis

Raman spectroscopy is a powerful tool to probe the structural and vibrational property of a material. Room

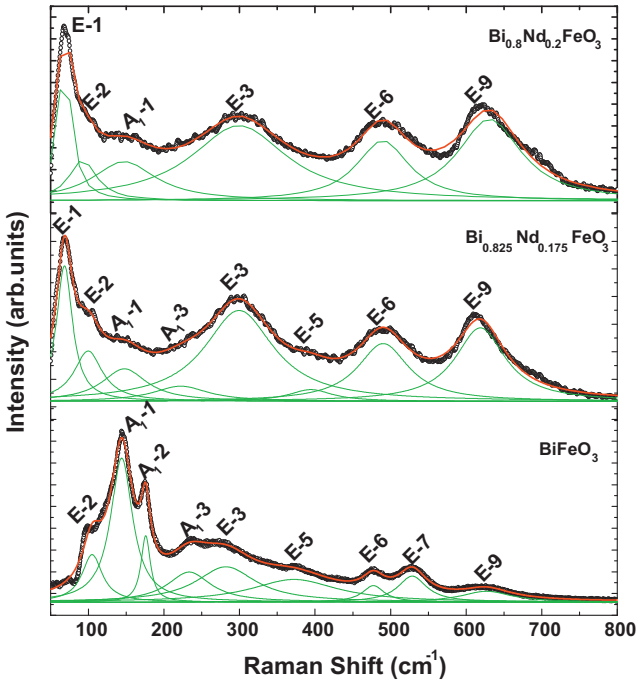

Fig. 4. Raman spectra for $Bi_{1-x}Nd_xFeO_3$ ($x = 0.0, 0.175, 0.20$) samples at room temperature with excitation wavelength of 488 nm.

temperature Raman spectra of BFO, BNFO-175, and BNFO-20 samples with excitation wavelength of 488 nm are shown in Fig. 4. It has been reported that BFO with distorted rhombohedral structure, *R*3*c* space group and 10 atoms in a unit cell of this structure yields 18 optical phonon modes and can be summarized using following irreducible representation: $\Gamma_{opt} = 4A_1 + 5A_2 + 9E$. According to group theory 13 observed modes ($\Gamma_{Raman,\ R3c} = 4A_1 + 9E$) are Raman active, whereas, $5A_2$ are Raman inactive modes [22,23]. The A_1-modes are associated with Fe ions and *E*-modes are associated with Bi ions. The dependence of mode positions on parent $BiFeO_3$ and Nd doped BFO are summarized in Table 5. For the comparison purpose the mode assignment of BFO and $Bi_{0.825}Nd_{0.175}FeO_3$ thin film is also included from the earlier reported data [22,24,25].

In present study, nine Raman active phonon modes of pure BFO sample including A_1-1, A_1-2, A_1-3, *E*-2, *E*-3, *E*-5, *E*-6, *E*-7, and *E*-9 modes at 144, 175, 232, 100, 279, 375, 477, 528, and 620 cm^{-1} are in good agreement with earlier reported bulk and thin film BFO [22,24]. The ferroelectricity of BFO generally originates from the stereochemical activity of the Bi ion lone pair electron that is mainly responsible for the change in both Bi–O covalent bonds. The six characteristic modes i.e. *E*-1, A_1-1, A_1-2, A_1-3, A_1-4, and *E*-2 are believed to be responsible for the FE nature of the bismuth ferrite samples. As evident from the X-ray diffraction the crystal symmetry varies from rhombohedral (*R*3*c*) to triclinic (*P*1) on subsequent Nd doping in the BFO samples. These changes in crystal structure are attributed to the *A*-site disorder created by Nd substitution, which leads to the shifting of Raman modes at higher frequencies with sudden disappearance of some modes (A_1-2 and *E*-7 in BNFO-175 and A_1-2, A_1-3, *E*-5, and *E*-7 in BNFO-20).

An additional *E*-1 mode at 68.27 and 75.34 cm^{-1} appears newly in Nd doped BFO samples, which is too weak to detect in pure BFO sample. These phenomena reflect the change of Bi–O covalent bonds with increasing doping concentration and induced ferroelectricity. The strong characteristic modes corresponding to Bi–O covalent bonds shift toward a higher wave number with increasing Nd content for BNFO-175 and BNFO-20 as compared to pure BFO. This can be attributed to the lower atomic weight of Nd^{3+} (144.24 g) compared to Bi^{+3} (208.98 g). Furthermore for Nd doped samples intensity of *E* modes increases whereas A_1 mode intensity decreases drastically. This may be due to the structural transformation from rhombohedral (*R*3*c*) to triclinic (*P*1) and account for the fact that Nd doping affect the *A* site in BFO.

4.4. Ferroelectric (P–E) properties

The room temperature ferroelectric hysteresis (*P*–*E*) loop for BFO, BNFO-175, and BNFO-20 compounds is shown in

Table 5
Comparison of Raman modes (cm^{-1}) from $Bi_{1-x}Nd_xFeO_3$ ($x = 0.0, 0.175, 0.20$) samples and the literature.

Raman modes (cm^{-1})	Present study			Literature		
	BFO	BNFO-175	BNFO-20	BFO Bulk (Kothari et al. [24])	BFO Thin film (Singh et al. [22])	BNFO Thin film (Yuan et al. [25])
A_1-1	143.97	147.58	151.21	135.15	136	144.3
A_1-2	175.92	–	–	167.08	168	165.2
A_1-3	233.37	222.24	–	218.11	212	229.2
A_1-4	–	–	–	430.95	425	–
E-1	–	68.27	75.34	71.39	77	–
E-2	104.97	105.63	107.51	98.36	275	271
E-3	281.09	299.36	304.02	255.38	335	306.8
E-4	–	–	–	283.0	363	
E-5	372.15	394.37	–	321.47	–	369.9
E-6	477.22	490.12	495.65	351.55	456	473.3
E-7	528.59	539.60	–	467.60	549	523.3
E-8	–	–	–	526.22		
E-9	626.86	619.66	622.94	598.84	597	620.3

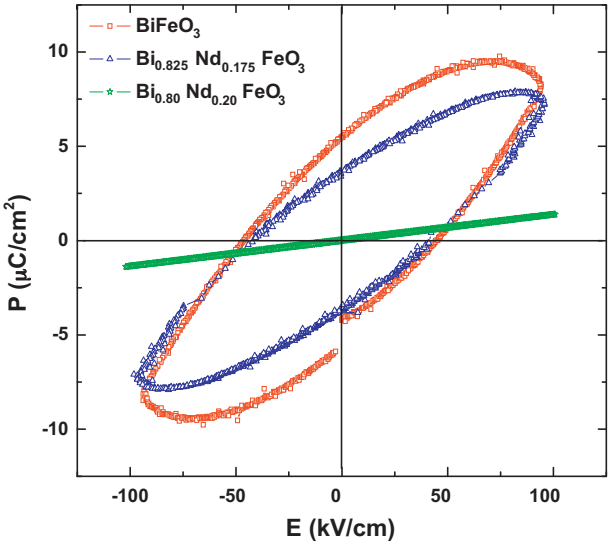

Fig. 5. The ferroelectric polarization hysteresis (P–E) loops of $Bi_{1-x}Nd_xFeO_3$ ($x = 0.0, 0.175, 0.20$) samples.

Fig. 5. It has been observed from the graph that BFO and BNFO-175 samples represent ferroelectric behavior whereas BNFO-20 sample represents paraelectric behavior. The spontaneous polarization ($2P_s$), remnant polarization ($2P_r$), and coercive (E_c) are about ~16 μc/cm^2, 11 μc/cm^2, and 44 kV/cm, respectively, for pure BFO. Whereas, for BNFO-175 compound the obtained value of $2P_s$, $2P_r$, and E_c are about 15 μc/cm^2, 7 μc/cm^2, and 40 kV/cm, respectively, under high electric field of ~95 kV/cm. The obtained ferroelectric hysteresis loop of BFO matches well with the earlier reported P–E measurement [26].

Furthermore, for paraelectric BNFO-20 sample the obtained values of $2P_s$ (~2.6 μc/cm^2) and $2P_r$ (~0 μc/cm^2) are found to be much lower than ferroelectric BFO and BNFO-175 even at a high field of 100 kV/cm. The lower P_r value of BNFO-20 relative to that of pure BFO despite of its higher applied electric field indicates that Nd doping degrades the ferroelectric nature. The obtained results account for the fact that stereochemical activity of the Bi lone pair electron plays a major role in ferroelectric to paraelectric transition. In the present case of BFO and BNFO-175 the Bi^{3+} lone pair electron hybridizes with empty p orbital of Bi^{3+} or an O^{2-} ion to form Bi–O covalent bonds ensuing the noncentrosymmetric distortion and ferroelectricity. Further increase of Nd concentration weakens the stereochemical activity and results in FE–PE transition.

5. Conclusions

Polycrystalline samples of $Bi_{1-x}Nd_xFeO_3$ ($x = 0.0, 0.175, 0.20$) were successfully prepared by chemical co-precipitation method. The effect of doping in the BFO compound on its structural and ferroelectric properties has been studied. X-ray diffraction confirms the formation of single phase with a structural transformation from rhombohedral ($R3c$) to triclinic structure ($P1$). All the three samples fitted with Rietveld refinement using FullPROF program revealed the existence of rhombohedral structure with space group $R3c$ for undoped $BiFeO_3$ and triclinic structure with space group $P1$ for Nd doped $BiFeO_3$ samples. The A site substitution of Nd^{3+} ion has shown to weaken the stereochemical activity of Bi lone electronic pair and Bi–O covalent bonds. Evolution of Raman spectra reveals the active phonon modes for all the samples and shows the FE–PE transformation because of doping concentration. Room temperature polarization hysteresis loop (P–E) also reveals the structural transformation showing the ferroelectric loop for BFO, BNFO-175 and paraelectric loop for BNFO-20.

Acknowledgements

Financial assistance from UGC, New Delhi is gratefully acknowledged. The authors wish to thank Dr. V.G. Sathe, Dr. M. Gupta and Dr. V.R. Reddy, UGC-DAE-CSR, Indore for caring out the Raman, XRD, and PE measurements.

References

[1] M. Fiebig, Revival of the magnetoelectric effect, J. Phys. D: Appl Phys. 38 (2005) R123.
[2] G. Catalan, J.F. Scott, Physics and applications of bismuth ferrite, Adv. Mater. 21 (2009) 2463–2485.
[3] J.B. Neaton, C. Ederer, U.V. Waghmare, N.A. Spaldin, K.M. Rabe, First-principles study of spontaneous polarization in multiferroic $BiFeO_3$, Phys. Rev. B 71 (2005) 014113.
[4] R. Seshadri, N.A Hill, Visualizing the role of Bi 6s lone pairs in the off-center distortion in ferromagnetic $BiMnO_3$, Chem. Mater. 13 (2001) 2892–2899.
[5] I. Sosnowska, T.P Neumair, Spiral magnetic ordering in bismuth ferrite, J. Phys. C: Solid State Phys. 15 (1982) 4835.
[6] W. Kaczmarek, Z. Pajak, Differential thermal analysis of phase transitions in $Bi_{1-x}La_xFeO_3$ solid solution, Solid State Commun. 17 (1975) 807–810.
[7] G.L. Yuan, S.W. Or, J.M. Liu, Z.G. Liu, Structural transformation and ferroelectromagnetic behavior in single-phase $Bi_{1-x}Nd_xFeO_3$ multiferroic ceramics, Appl. Phys. Lett. 89 (2006) 052905.
[8] G.L. Yuan, S.W. Or, Enhanced piezoelectric and pyroelectric effects in single-phase multiferroic $Bi_{1-x}Nd_xFeO_3$ ($x = 0$–0.15) ceramics, Appl. Phys. Lett. 88 (2006) 062905.
[9] N. Jeon, D. Rout, W. Kim, S.L. Kang, Enhanced multiferroic properties of single-phase $BiFeO_3$ bulk ceramics by Ho doping, Appl. Phys. Lett. 98 (2011) 072901.
[10] H.M. Rietveld, Line profiles of neutron powder-diffraction peaks for structure refinement, Acta Crystallogr. 22 (1967) 151–152.
[11] H.M. Rietveld, A profile refinement method for nuclear and magnetic structures, J. Appl. Crystallogr. 2 (1969) 65–71.
[12] S.K. Pradhan, S. Bid, M. Gateshki, V. Petkov, Microstructure characterization and cation distribution of nanocrystalline magnesium ferrite prepared by ball milling, Mater. Chem. Phys. 93 (2005) 224.
[13] S. Bid, S.K. Pradhan, Preparation and microstructure characterization of ball-milled ZrO_2 powder by the Rietveld method: monoclinic to cubic phase transformation without any additive, J. Appl. Crystallogr. 35 (2002) 517.
[14] J. Rodriguez-Carvajal, Recent advances in magnetic structure determination by neutron powder diffraction, Physica B 192 (1993) 55.
[15] R.A. Young, D.B. Wiles, Application of the Rietveld methods for structure refinement with powder diffraction data, Adv X-ray Analysis 24 (1980) 1–23.
[16] R.A. Young, D.B. Wiles, Profile shape functions in Rietveld refinements, J. Appl. Cryst. 15 (1982) 430–438.

[17] R.D. Shannon, Revised effective ionic radii and systematic studies of interatomic distances in halides and chalcogenides, Acta Crystallogr. A 32 (1976) 751–767.

[18] A. Jaiswal, R. Das, K. Vivekanand, P.M. Abraham, S. Adyanthaya, P. Poddar, Effect of reduced particle size on the magnetic properties of chemically synthesized $BiFeO_3$ nanocrystals, J. Phys. Chem. C 114 (2010) 2108.

[19] G.L. Yuan, K.Z. Baba-Kishi, J.-M. Liu, S.W. Or, Y.P. Wang, Z.G. Liu, Multiferroic properties of single-phase $Bi_{0.85}La_{0.15}FeO_3$ lead-free ceramics, J. Am. Ceram. Soc. 89 (2006) 3136–3139.

[20] N. Kumar, N. Panwar, B. Gahtori, N. singh, H. Kishan, V.P.S. Awana, Structural, dielectric and magnetic properties of Pr substituted $Bi_{1-x}Pr_xFeO_3$ ($0 \leq x \leq 0.15$) multiferroic compounds, J. Alloys Compd. 501 (2010) 129.

[21] V.M. Goldschmidt, Die Gesetze der Krystallochemie, Naturwissenschaften 14 (1926) 477.

[22] M.K. Singh, H.M. Jang, S. Ryu, M.H. Jo, Polarized Raman scattering of multiferroic $BiFeO_3$ epitaxial films with rhombohedral R3c symmetry, Appl. Phys. Lett. 88 (2006) 42907.

[23] R. Haumont, J. Kreisel, P. Bouvier, F. Hippert, Phonon anomalies and the ferroelectric phase transition in multiferroic $BiFeO_3$, Phys. Rev. B 73 (2006) 132101.

[24] D. Kothari, V.R. Reddy, V.G. Sathe, A. Gupta, A. Banerjee, A.M. Awasthi, Raman scattering study of polycrystalline magnetoelectric $BiFeO_3$, J. Magn. Magn. Mater. 320 (2008) 548.

[25] G.L. Yuan, S.W. Or, H.L.W. Chan, Z.G. Liu, Reduced ferroelectric coercivity in multiferroic $Bi_{0.825}Nd_{0.175}FeO_3$ thin film, J. Appl. Phys. 101 (2007) 024106.

[26] Y.P. Wang, G.L. Yuan, X.Y. Chen, J.-M. Liu, Z.G. Liu, Electrical and magnetic properties of single-phased and highly resistive ferroelectromagnet $BiFeO_3$ ceramic, J. Phys. D: Appl. Phys. 39 (2006) 2019.